INTERNATIONAL JOURNAL OF AUTOMOTIVE AND MECHANICAL ENGINEERING
ISSN: 2229-8649 e-ISSN: 2180-1606
VOL. 21, ISSUE 1, 2024, 11166 – 11175
DOI: https://doi.org/10.15282/ijame.21.1.2024.17.0863

RESEARCH ARTICLE

Discharge and Thermal Distribution Characteristics of Electric Vehicle Battery Pack in Closed Circuit System

D. H. Arthanto[1]*, B. Nuryadin[2], Fitrianto[3], K. P. Sumarah[3], M. P. Helios[3], H. Sutriyanto[3] and A. Maswan[3]

[1]Research Center for Accelerator Technology, Nuclear Energy Research Organization (ORTN), National Research and Innovation Agency (BRIN), 55281, Sleman, Yogyakarta, Indonesia
[2]Ministry of Energy and Mineral Resources Republic of Indonesia, Jakarta Pusat 10110, Indonesia
[3]Research Center for Energy Conversion and Conservation, Energy and Manufacturing Research Organisation (OREM), National Research and Innovation Agency (BRIN), 15314, Tangerang Selatan, Banten, Indonesia

ABSTRACT - This paper presents an experimental study of the depth of discharge (DOD) and temperature distribution characteristics at different locations of the lithium-ion battery (LIB) pack in the closed circuit system. Three different discharge power setups i.e., 600 W, 800 W, and 1000 W are prepared for investigating the depth of discharge and temperature characteristics of commercial LIB. Voltage measurement was implemented to achieve the DOD curve, while thermocouple measurement was used to identify real-time temperature at four different locations of the LIB. As a result, internal resistance and discharging time tend to be increased, while the voltage and current decline linearly from 0% to 80% of LIB capacity. Discharge power greatly affected the four variables when the process continued to the 10% cut-off voltage. Furthermore, the heat generation of the LIB caused a rise in temperature on its surface. The highest temperature was identified on the LIB cell surface followed by an air gap, internal surface casing, and external surface casing temperature. Among all locations, the real-time temperature on the LIB surface operated close to the upper limit of optimum temperature. Due to that reason, increasing of discharge power should be maintained to extend battery cycle life as well as to prevent battery failure. The high-temperature difference between the LIB surface and air gap during the discharging process indicated that there is required heat transfer enhancement.

ARTICLE HISTORY
Received : 27th Dec. 2022
Revised : 11th Jan. 2024
Accepted : 26th Feb. 2024
Published : 20th Mar. 2024

KEYWORDS
Depth of discharge
Temperature distribution
Lithium-ion battery
Closed circuit system

1.0 INTRODUCTION

Nowadays, greenhouse gas emissions and hydrocarbon leaks lead to climate change phenomena and harmful situations in the future. As a critical issue, net-zero emission (NZE) is the primary goal of achievement for many countries by 2050, especially Indonesia [1]. The industrial energy sector was the largest emission source, contributing 43.83% of the total emissions in 2019, followed by the transportation sector at about 24.64% [2]. In the case of transportation, the shift from traditional fossil-fueled vehicles to electric vehicles was declared to support the NZE blueprint of the Indonesian transportation sector [3].

Referring to global demand, electric car trading grew two times from 2020 to 2021, reaching about 8.57% [4]. Most of these electric vehicles are complemented with lithium-ion batteries (LIBs) as efficient and effective energy storage. It becomes the best option compared to other batteries due to its lightweight, high specific energy, energy density, and superior capacity relative to other rechargeable battery types [5]. Despite the advantages, scrutiny of lithium-ion batteries (LIBs) during operation cannot be detached from thermal aspects. Improper thermal treatment can cause thermal runaway, leading to chemical leakage, explosions, and fires [6]. The main challenges for maintaining Li-ion battery safety and high performance are strongly related to battery thermal management [7]. The optimal working temperature for LIBs is between 10°C and 50°C [8], 15°C up to 35°C [9], or 20°C up to 40°C [10].

Charging and discharging processes are common procedures to test LIBs' ability. Most research focuses on LIBs' ability to use an open circuit system [11]–[17]. Kurzweil et al. investigated the state of charge (SOC) and the state of health (SOH) of five types of LIBs. They introduced differential capacity as a tool to indicate upcoming heat events and deep discharge. The study stated that there is no general formula able to display and predict SOC and SOH in all system states [11]. Verasamy et al. developed a battery management system with an intelligent charge control scheme for a single LIB. Their study investigated the optimum charging and discharging characteristics of the storage system but lacked temperature analysis. They claimed that the proposed system could save energy and prolong battery life [12]. Srinivasan et al. implemented an advanced battery internal temperature sensor-based (BITS) system. It connected the discharge process to the temperature measurement of anode LIBs. Their work claimed that it successfully monitors anode temperature and other parameters in real-time, recording heat- and discharge-induced events affecting the anode and the solid electrolyte interphase (SEI) [14]. Sumarah et al. investigated the effect of torque variation on LIB pack temperature. Their study revealed that temperature distribution on the surface of the LIB pack case is not uniform. The highest temperature was identified at 100% torque, and their research did not investigate the discharge curve of the LIB pack

***CORRESPONDING AUTHOR | D. H. Arthanto** | ✉ dwi.handoko.arthanto@brin.go.id

[16]. However, there is still a chance to improve previous studies since the study was limited to the single LIB and did not entirely focus on thermal distribution.

Based on the author's current knowledge of lithium-ion battery technology scope, proficient management of thermal conditions stands as a pivotal factor in ensuring the reliability, safety, and operational efficiency of electrochemical energy storage systems. As demand for lithium-ion batteries continues its rapid ascent across diverse applications such as electric vehicles and renewable energy integration, the need to elucidate and optimize the thermal behavior of LIBs in response to variable load profiles becomes increasingly imperative. This research is dedicated to conducting a comprehensive examination of thermal management systems specifically designed for LIBs for domestic two-wheel electric vehicles in Indonesia, with a pronounced focus on their dynamic response to varying DC load conditions, i.e., resistive and inductive loads. An experimental study has been conducted to achieve the characteristics of the temperature profile of the discharge power and to distinguish temperature distribution temperatures in the location of the LIB pack. As a sample, a commercial LIB pack with a square case of domestic electric motorcycles in Indonesia is selected as a specimen for the measurement. All temperatures in various locations, internal and external battery cases, are measured, as well as the current and voltage. Our research plays a key role in enhancing energy storage technologies by offering detailed insights into thermal dynamics and suggesting creative solutions to address issues caused by load fluctuations. The experiment's results will be used to enhance the design of a hybrid passive cooling system for the LIB battery through CFD simulation and optimizing heat dispersion on the surface cover of electric vehicle batteries.

2.0 METHODOLOGY

An experimental study concerning the temperature characteristic distribution of LIB under discharging conditions was conducted in Building No. 232 at the Laboratory for Thermodynamics, Engine, and Propulsion Technology, National Research and Innovation Agency, Serpong, Indonesia.

2.1 Experimental Setup

There are many models of electric motorcycle battery capacity in the Indonesian EV market. According to research collaboration with a domestic EV company competing in the battery market, it became essential to test the durability and performance of the battery in the laboratory. As samples, a LIB with a capacity of 82 V and 20 Ah, along with its dimensions (length: 125 mm, width: 125 mm, and height: 385 mm), were prepared during testing. The battery pack is composed of four modules of cylindrical battery cells, each containing 20 cells of LG INR21700 5000 mAh. The energy density of the battery pack was approximately 10.68 Wh/g. The battery cells feature an NMC 811 formulation as the cathode and Graphite-SiOx as the anode. The sample not only has the highest voltage and lightest weight among motorcycle batteries but also a unique arrangement of battery modules in the Indonesia EV market. Hence, the present test results are essential for developing better heat transfer and lighter battery casing.

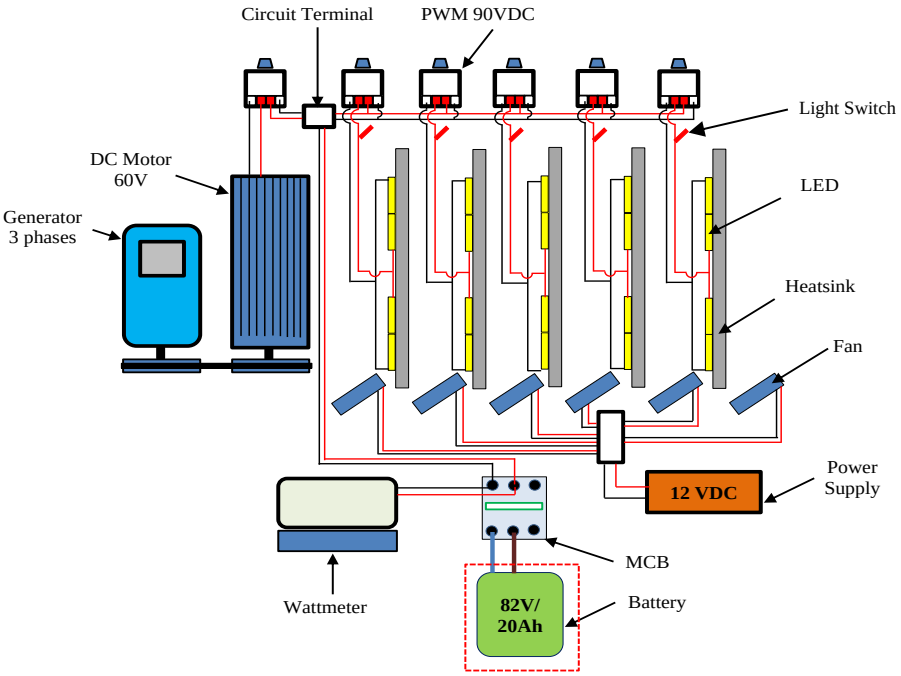

(a)

Figure 1. Closed-circuit discharger system: (a) schematic of wiring diagram

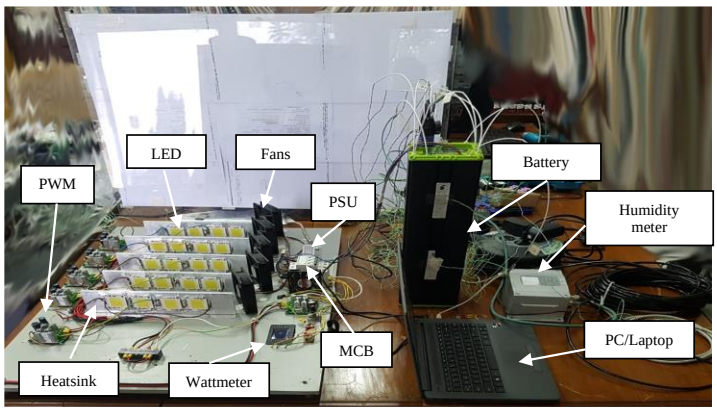

(b)

Figure 1. (cont.) (b) experimental setup

Figure 1 depicts the complete schematic of the experiment for discharging battery power. The discharger system was constructed based on the DC load method with closed circuit voltage (CCV). The discharger apparatus consisted of several electrical components, including a power supply, pulse width modulation (PWM), fan, LED, and DC motor. The battery is connected to the main circuit breaker (MCB), and the power is linked to the circuit terminal. There are two electric transmission lines that distribute to six PWMs and a DC motor as input. The main voltage is adjusted from 82 V to 34 V for the LED and from 82 V to 60 V for the DC motor respectively.

In the case of the LED, four 100-watt LEDs are wired in series and parallel to achieve a higher current in each LED circuit. Each LED is installed on an aluminum heatsink to reduce heat dissipation, which is required to be maintained under the operating temperature of the LED. Hence, five high-speed fans are placed to circulate airflow on the heatsink continuously. A 12 VDC power supply is used to power each fan in parallel. Later, the DC motor is coupled with three-phase generators via a v-belt. All the battery capacity and other parameters (voltage, current, power, watt, current flow, resistance) were monitored on the wattmeter display (PZM-015 50A).

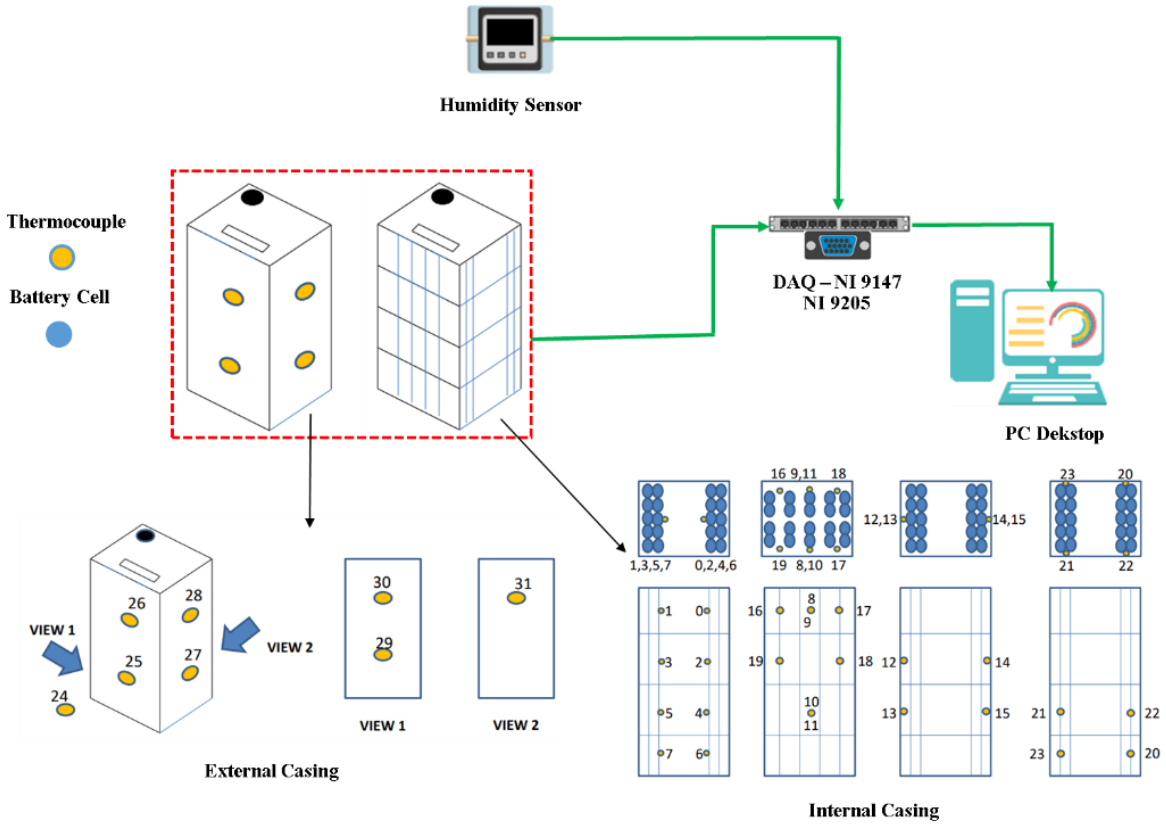

Figure 2. Temperature sensor installation in the external and internal casing

Figure 2 shows the locations of thirty-two thermocouples in the external and internal battery casing. The thermocouples used in this research include probe type, surface type, and plate type. Sixteen surface thermocouples are installed on the internal battery cell surface. Later, four plate-type thermocouples are installed on the internal casing surface, and four thermocouples with 1 mm probes are mounted to measure air temperature in the gap. To minimize

measurement errors caused by heat from the inner surface of the battery casing and the surface of the battery cell, each of the eight thermocouples is inserted into 2 mm acrylonitrile butadiene styrene (ABS) tubes. Additionally, seven surface thermocouples are affixed to the external surface of the battery casing, and a thermocouple is fixed to measure ambient temperature, following our previous method [8]. The details of the thermocouple positions are listed in Table 1. Moreover, a humidity sensor is used to measure the humidity and dry bulb temperature of the environment. All data are recorded simultaneously using NI 9147 with NI modules 9205 and 9206 before being transferred to the PC desktop.

Table 1. Detail of temperature sensor number and location in the installation

Location	Thermocouples Number	Type	Accuracy (°C)	Resolution (°C)
Internal battery cell surface	0 – 11; 16-19	Surface	± 0.25	0.01
Internal casing surface	12-15	Plate-	± 0.25	0.01
The air gap between the internal casing and the battery cell	20-23	Probe	± 0.25	0.01
Ambient air	24	Surface	± 0.25	0.01
External casing surface	25-31	Surface	± 0.25	0.01

2.2 Experimental Procedure

The testing equipment was designed to observe the charging and discharging process in the lithium-ion battery. The equipment utilized electrical load, with the first being a resistive load using 100-watt LED lamps connected in series and parallel, with 4 LED lights per line for a total of 5 lines. The second method involved an inductive load using a 720-watt DC motor. The output voltage of the LED lamps and DC motor was controlled by the PWM, which manipulated the pulse width contained in a square wave. Consequently, the power of the LED lamps and the rotational speed of the DC motor were regulated smoothly. As the first procedure, the MCB and the fan system were turned on, and the condition of each lamp cooling fan was checked. Subsequently, the light switch, as shown in Figure 1, was gradually pressed to activate the resistive load, followed by turning on the DC motor load switch as an inductive load. Both loads were used in this study. Three different load values of power output were prepared, ranging from 600 W to 1000 W, with a 200 W increment maintained. The experiment matrix is tabulated in Table 2.

Table 2. Matrix of the experiment

No.	Discharge power (W)	Configuration	Measured variables
1	600	3 rows LED + DC motor	Resistance, current, voltage and temperature
2	800	4 rows LED + DC motor	Resistance, current, voltage and temperature
3	1000	5 rows LED + DC motor	Resistance, current, voltage and temperature

Later, the temperature of the battery was measured simultaneously by thermocouple and recorded by data acquisition during the discharging process. Eventually, the discharging of the LIB was stopped when the battery capacity reached 10% or approximately 62 V cut-off voltage, indicating the depth of discharge (DOD) limit of the battery. The state of charge (SOC) and the depth of discharge (DOD) are the most important parameters for batteries. Generally, the SOC represents the ratio of its current capacity $\left(Q_{(t)}\right)$ to the nominal capacity (Q_n). Meanwhile, the DOD is the percentage of electric charge released from the fully charged battery. Both SOC and DOD formulations are expressed as follows [18], [19].

$$SOC_{(t)} = \frac{Q_{(t)}}{Q_n} \times 100\% \tag{1}$$

or

$$DOD_{(t)} = 1 - SOC_{(t)} \tag{2}$$

Along with that, the analysis of experimental uncertainty is imperative to obtain a proper elucidation of experimental results. The uncertainty of measurement of the temperature sensor is calculated using the standard procedure ASME PTC 19.1-2005 [20]. Additionally, the uncertainty of measurement of the temperature sensor and parameter is calculated by following the procedure given by Kee et al. [21]. The combined uncertainty $(U_{tot.})$ of measured temperature consists of the uncertainty of the instrument $(U_{inst.})$, the uncertainty of Reference Junction Compensation (U_{RJC}), and the uncertainty of random fluctuation $(U_{rand.})$, which is calculated by the equation as follows:

$$U_{tot.} = \sqrt{(U_{inst.})^2 + \left(U_{RJC}\right)^2 + (U_{rand.})^2} \tag{3}$$

Table 3. The overall uncertainty of measured temperature

Location	$U_{inst.}, °C$	$U_{RJC}, °C$	$U_{rand.}, °C$	$U_{tot.}, °C$
Internal battery cell surface	$\pm$ 0.25	$\pm$ 0.34	±0.011 - ±0.014	0.42223
Internal casing surface	$\pm$ 0.25	$\pm$ 0.34	±0.012 - ±0.014	0.42221
The air gap between the internal casing and the battery cell	$\pm$ 0.25	$\pm$ 0.34	±0.011 - ±0.013	0.42218
Ambient air	$\pm$ 0.25	$\pm$ 0.34	±0.013 - ±0.016	0.42225
External casing surface	$\pm$ 0.25	$\pm$ 0.34	±0.012 - ±0.015	0.42225

The combined uncertainty result of measured variables in percentage is summarized in Table 3. The uncertainty of temperature measurement results ensures that the thermocouples used in the present study are well-calibrated.

3.0 RESULTS AND DISCUSSION

3.1 Deep of Discharge (DOD)

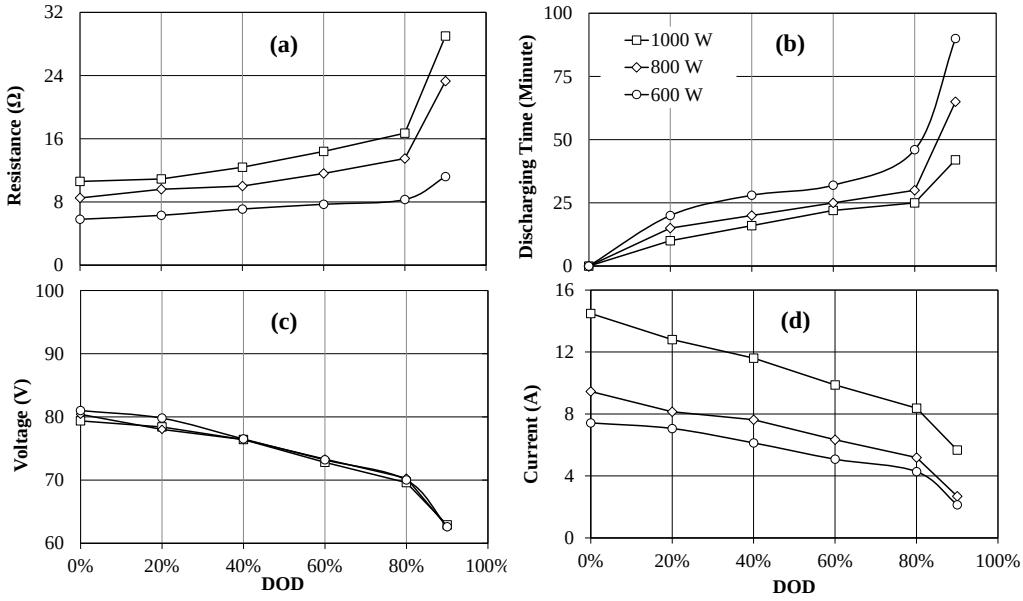

Figure 3. Deep of Discharge Curve; (a) Resistance, (b) Discharging time, (c) Voltage and (d) Current

Figures 3(a) and 3(b) depict similar trends at different power discharges. Both resistance and discharging time slightly increased from DOD 0% to 80% for each power discharge, then increased sharply when the DOD was over 80%. The higher resistance occurred at high-power discharge, affecting the increase of the current discharge rate. Consequently, the discharging time of the LIB becomes shorter, and vice versa. In addition, Figures 3(c) and 3(d) show the opposite curve compared to others. Initially, both the voltage and current have a sloping drop from the initial stage. Both voltage and current of the LIB decrease linearly from 0% to 80%, while both variables decline sharply at DOD over 80%. According to Ohm's law, the reason for the voltage drop is due to capacity depletion and increasing total resistance in the closed circuit.

Deep discharging a battery means using a significant portion of its stored energy capacity. As a result, the battery's capacity decreases substantially. If the discharge continues beyond the recommended depth of discharge (DoD) for a particular battery type, it can lead to a complete depletion of the available energy. Moreover, the internal resistance of a battery increases as it discharges, leading to heat generation. In a deep discharge scenario, this heat production can be more pronounced and potentially result in overheating if not properly managed. Further, uncontrolled DOD can trigger chemical reactions within the battery cells. These reactions can include the formation of undesirable compounds, such as lithium plating in lithium-ion batteries, which can reduce the battery's capacity and overall performance.

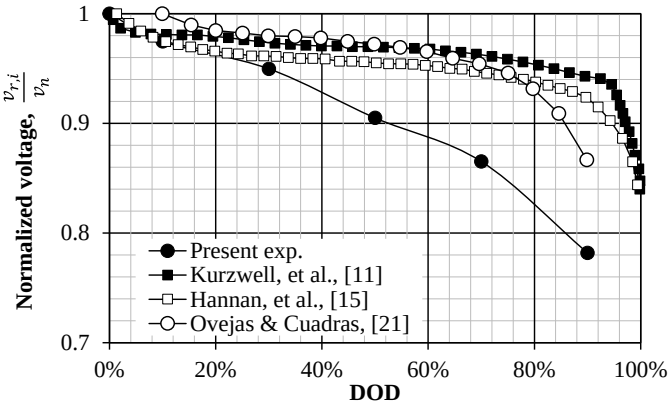

Figure 4. Comparison of the present experiment and hysteresis voltage discharge curves

Figure 4 shows the present discharge curve compared to the hysteresis of discharge curves of LIB cells from other authors in terms of normalized voltage [11], [15], [22]. It is defined as the ratio between the remaining voltage ($v_{r,i}$) and the nominal voltage ($v_{n.}$). The graph of the experiment is slightly lower than other curves. This is because of the different discharge systems and battery configurations. The present experiment used a closed-circuit system arranged by four modules, while the reference curve used an open-circuit system with a single battery. The experiment result has higher resistance than others because the configuration has not only internal resistance but also load resistance. However, the results show a good trend compared to the hysteresis discharge curves of LIB.

3.2 Temperature Distribution Characteristic

As a battery undergoes a discharge cycle, one noteworthy phenomenon is the increase in temperature, especially when approaching higher levels of Depth of Discharge (DOD). This rise in temperature is primarily a result of the increased internal resistance within the battery. As the battery discharges, its internal components, including the electrolyte and electrodes, experience higher current flows and greater electrical resistance. This resistance generates heat as a byproduct, leading to a gradual elevation in temperature. The effect is more pronounced during deep discharges and high-power discharges.

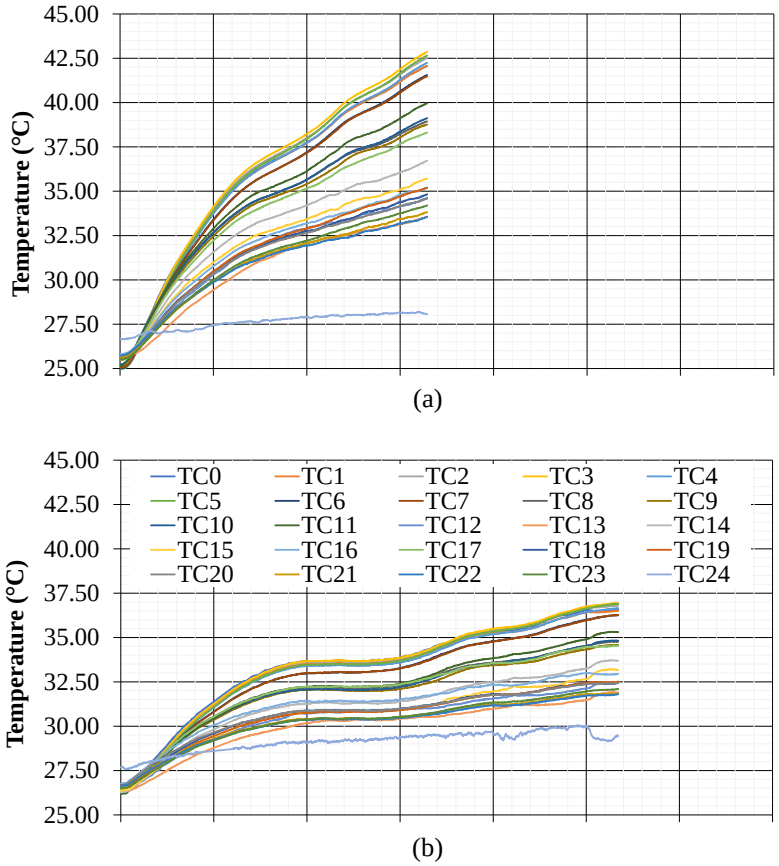

Figure 5. Transient temperature profile at different power outputs: (a) 1000 W, (b) 800 W

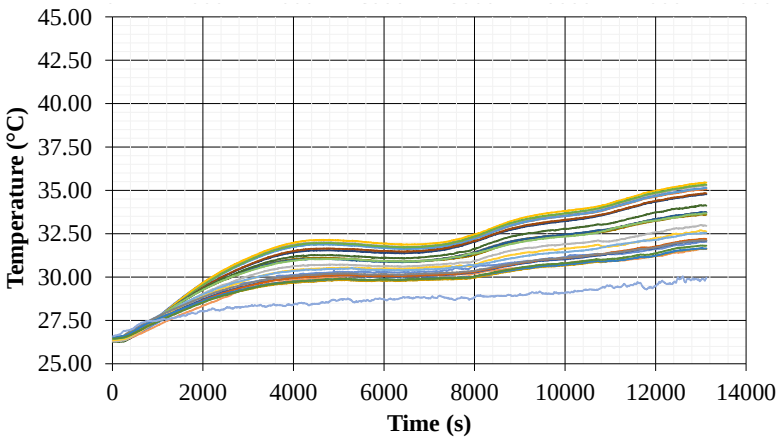

(c)

Figure 5. (cont.) (c) 600 W

Figure 5 shows the temperature profile distribution of the battery in the internal battery casing. The temperature increased linearly during discharge power, leading to an increase in temperature in each location. In the present measurement, each power output is calculated at about 1003.52 W, 759.78 W, and 601.02 W, respectively. There is a 5.13% error between the experiment setup and the measurement for the 800 W load. Later, the higher the power discharge, the shorter the discharging time. Decreasing the power output by 200 W extends the operating time of the battery by about one hour.

Figure 6 depicts the transient temperature distribution in each location of thermocouples for power output 1000 W. Figure 6(a) illustrates that the temperature surface of the LIB cell tends to increase sharply compared to other locations. Some of the battery cell's temperatures are relatively high compared to the optimum battery temperature recommendation of 15 °C up to 35 °C [9] or 20 °C up to 40 °C [10]. The temperature difference (ΔT) between the lowest and highest temperatures of the battery cell at the end of discharge was about ±9°C. It indicates there is an imbalance of discharge current flow in each LIB module or cell, which affects the heat generation in the LIB cell.

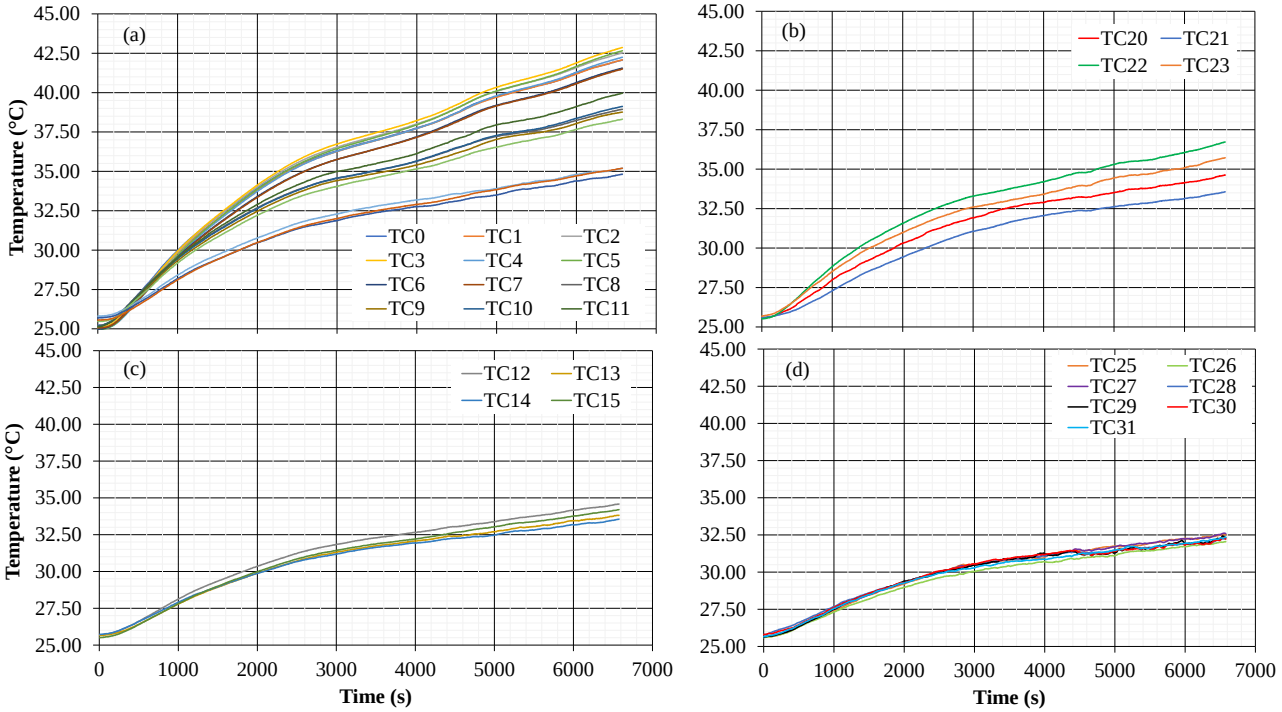

Figure 6. Transient temperature profile at different locations for 1000 W: (a) internal battery cell surface; (b) air gap between internal surface casing and battery cell; (c) internal surface casing, (d) external surface casing

Figure 6(b) shows the temperature of the air gap. Since a tiny gap appears between the LIB cell's internal surface casing, heat generation moves as convective flow. Due to the low thermal conductivity of the air gap, heat absorption is not well utilized. The ΔT between the lowest and highest air gap temperature was about 3°C. Similar convection heat transfer has also occurred from the air gap to the internal surface casing. Figure 6(c) depicts that the internal surface casing temperature ranged from 33.5°C to 34.5°C. It is higher by 1 to 2°C than the external surface casing temperature, as shown in Figure 6(d). Even though the present results of Figure 6(d) show the same trend compared to our previous

results, which used torque as the load [8]. The external surface casing temperature and discharge duration time of the present experiment are lower than 10°C and two times longer than the previous study. This was caused by the power discharged by the dynamometer being two times the maximum power in the present experiment. Reducing the power output of discharge in the present study was intended to avoid excessive heat generation, which could accelerate aging, potentially lead to capacity loss, and reduce cycle life. Consequently, precise thermal management systems and controls are essential to ensure that the battery operates within its recommended temperature range, optimizing its overall performance and longevity.

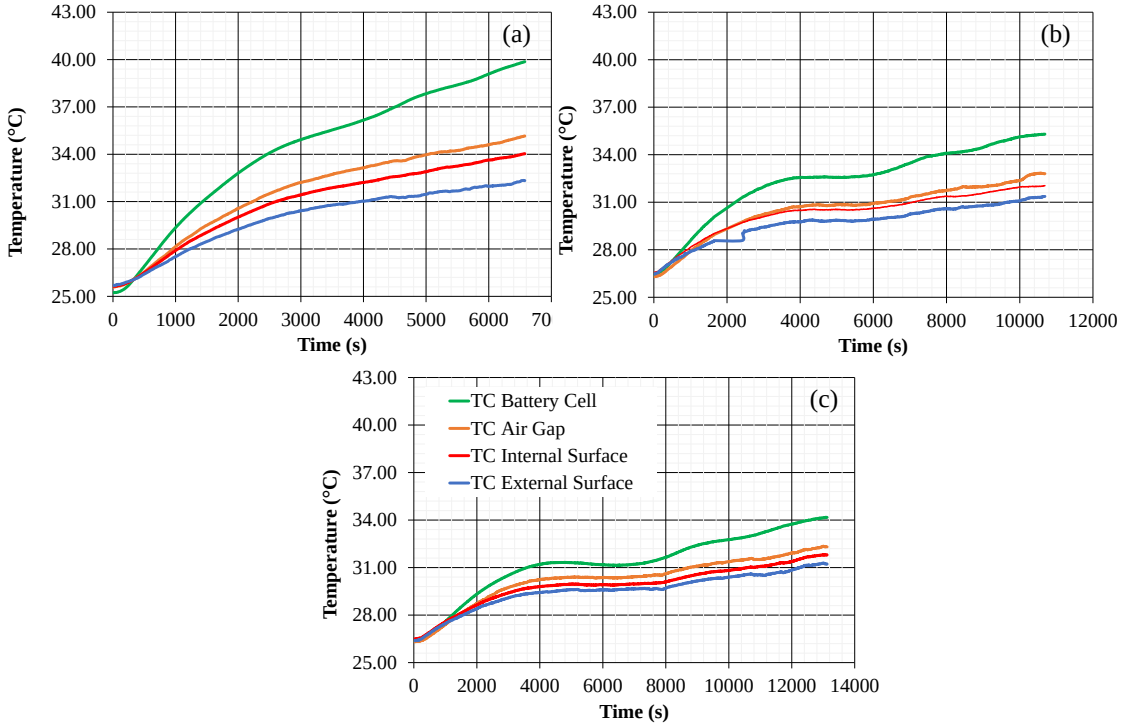

Figure 7. Average transient temperature profile at a different location: (a) 1000 W, (b) 800 W, & (c) 600 W

Figure 7 illustrates the average transient temperature among each position for three different discharged powers. The temperature trend is observed to increase for all locations. However, the temperature of the battery cell at 1000 W is close to 40°C, as shown in Figure 7(a). It indicates that it is almost at the upper limit of the optimum temperature for LIBs. In addition, Figures 7(b) and 7(c) show that the temperature at the different locations for 600 W and 800 W is still within the optimal range of LIB temperature. In essence, increasing the discharge power above 1000 W might generate a temperature on the surface of the LIB cell beyond the optimum range and cause an anode-electrolyte exothermic reaction [14].

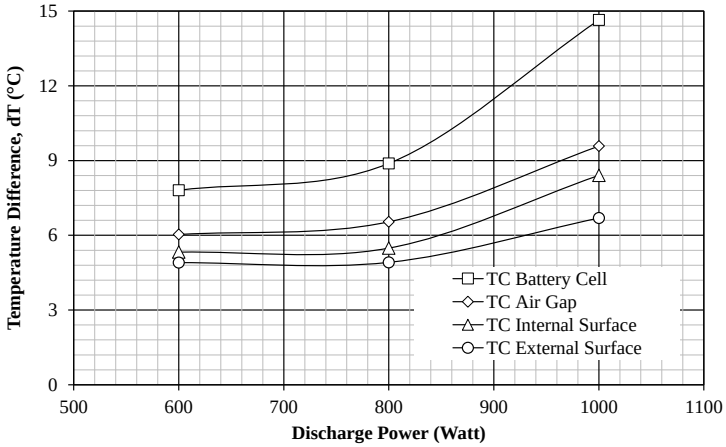

Figure 8. Temperature difference (ΔT) at different discharge power

Figure 8 depicts that increasing discharge power increases all temperatures in each location. The temperature of the air gap, internal surface, and external surface slightly increases from about 1°C to 3°C. The ΔT in the surface LIB is the highest among other locations, and the 1000 W discharge power produces a temperature difference close to 15°C. Afterward, the air gap between the battery module and the casing surface could act as an isolator medium during heat generation. This can be identified from the temperature difference among the locations. A higher temperature difference

indicates that the heat transfer from the inside to the outside of the LIB pack did not perform well. Hence, characterizing the temperature of the LIB pack is required to achieve a long lifespan under optimum conditions.

4.0 CONCLUSIONS

A study of the depth of discharge (DOD) and temperature characteristics at different locations of the LIB pack was conducted experimentally. Three different discharge power setups, i.e., 600 W, 800 W, and 1000 W, were prepared to investigate the depth of discharge and temperature characteristics of commercial LIB. According to the DOD curve, internal resistance and discharging time tend to increase, while the voltage and current decline linearly from 0% to 80% of LIB capacity. Similarly, DOD above 80% affected all four variables due to low capacity.

In summary, increasing the discharge power sharply reduced the battery capacity as well as discharging time. Consequently, the heat generation of the battery cell caused a rise in temperature on its surface. The highest temperature identified on the LIB cell surface was about 40°C at 1000 W discharge power, followed by an air gap, internal surface casing, and external surface casing temperature. Among all locations, the real-time temperature on the LIB surface operated close to the upper limit of the optimum temperature. Due to this reason, the use of discharge power over 1000 W should be maintained to extend battery cycle life as well as to prevent battery failure.

Furthermore, the high-temperature difference between the LIB surface and air gap during the discharging process indicated that there may be a problem in heat transfer. Since there is no ventilation in the LIB case, additional heat transfer area and medium are required as further solutions. This experimental study can be used to develop a proven battery thermal management system to prevent thermal runaway in batteries. Furthermore, the CFD approach is proposed to optimize heat transfer in the battery.

5.0 ACKNOWLEDGEMENT

The authors acknowledge the facilities, scientific and technical support from the Laboratory of Thermodynamics, Engine, and Propulsion Technology through E-Layanan Sains and a research grant from the Research Organization for Electronics and Informatics, National Research, and Innovation Agency, Indonesia.

6.0 REFERENCES

[1] F. D. B. Albuquerque, M. A. Maraqa, R. Chowdhury, T. Mauga, and M. Alzard, "Greenhouse gas emissions associated with road transport projects: Current status, benchmarking, and assessment tools," *Transportation Research Procedia*, vol. 48, pp. 2018–2030, 2020.

[2] Pusat Data dan Teknologi Informasi Energi dan Sumber Daya Mineral, "Inventarisasi Emisi GRK Bidang Energi," Jakarta, 2020. Accessed: Dec. 21, 2022. [Online]. Available: https://www.esdm.go.id/assets/media/content/content-inventarisasi-emisi-gas-rumah-kaca-sektor-energi-tahun-2020.pdf

[3] Presiden Republik Indonesia, "Peraturan Presiden Nomor 55 Tahun 2019 Tentang Percepatan Program Kendaraan Bermotor Listrik," no. 008553, pp. 1–6, 2019, Accessed: Dec. 21, 2022. [Online]. Available: https://jdih.esdm.go.id/storage/document/-Perpres Nomor 55 Tahun 2019.pdf

[4] IEA, "Global EV Outlook 2022 - Securing supplies for an electric future," *Glob. EV Outlook 2022*, p. 221, 2022, Accessed: Sep. 17, 2023, [Online]. Available: https://iea.blob.core.windows.net/assets/ad8fb04c-4f75-42fc-973a-6e54c8a4449a/GlobalElectricVehicleOutlook2022.pdf

[5] G. P. Nayaka, Y. Zhang, P. Dong, D. Wang, Z. Zhou, J. Duan, X. Li, Y. Lin, Q. Meng, K.V. Pai, J. Manjanna, and G. Santhosh, "An environmental friendly attempt to recycle the spent Li-ion battery cathode through organic acid leaching," *Journal of Environmental Chemical Engineering*, vol. 7, no. 1, p. 102854, 2019.

[6] W. Liu, T. Placke, and K. T. Chau, "Overview of batteries and battery management for electric vehicles," *Energy Reports*, vol. 8, pp. 4058–4084, 2022.

[7] W. E. Org, M. Hu, J. Wang, C. Fu, D. Qin, and S. Xie, "Study on Cycle-Life Prediction Model of Lithium-Ion Battery for Electric Vehicles," *International Journal of Electrochemical Science*, vol. 11, no. 1, pp. 577–589, 2016.

[8] Z. Rao, Z. Qian, Y. Kuang, and Y. Li, "Thermal performance of liquid cooling based thermal management system for cylindrical lithium-ion battery module with variable contact surface," *Applied Thermal Engineering*, vol. 123, pp. 1514–1522, 2017.

[9] W. Liu, Z. Jia, Y. Luo, W. Xie, and T. Deng, "Experimental investigation on thermal management of cylindrical Li-ion battery pack based on vapor chamber combined with fin structure," *Applied Thermal Engineering*, vol. 162, p. 114272, 2019.

[10] F.Yi, Jiaqiang E, B. Zhang, H. Zuo, K. Wei, J. Chen, H. Zhu, H. Zhu, and Y. Deng, "Effects analysis on heat dissipation characteristics of lithium-ion battery thermal management system under the synergism of phase change material and liquid cooling method," *Renewable Energy*, vol. 181, pp. 472-489, 2022.

[11] P. Kurzweil, W. Scheuerpflug, B. Frenzel, C. Schell, and J. Schottenbauer, "Differential capacity as a tool for SOC and SOH estimation of lithium ion batteries using charge/discharge curves, cyclic voltammetry, impedance spectroscopy, and heat events: A tutorial," *Energies*, vol. 15, no. 13, p. 4520, 2022.

[12] M. Verasamy, M. Faisal, P. J. Ker, and M. A. Hannan, "Charging and discharging control of Li-Ion battery energy management for Electric vehicle application," *International Journal of Engineering and Technology*, vol. 7, no. 4, pp. 482–486, 2018.

[13] T. Katrašnik, I. Mele, and K. Zelič, "Multi-scale modelling of Lithium-ion batteries: From transport phenomena to the outbreak of thermal runaway," *Energy Conversion and Management*, vol. 236, p. 114036, 2021.

[14] R. Srinivasan, P. A. Demirev, and B. G. Carkhuff, "Early-stage heat- and discharge-induced transformations in a lithium-ion cell monitored by an advanced battery management system," *Journal of The Electrochemical Society*, vol. 169, no. 2, p. 020522, 2022.

[15] M. A. Hannan, M. M. Hoque, A. Hussain, Y. Yusof, and P. J. Ker, "State-of-the-Art and Energy Management System of Lithium-Ion Batteries in Electric Vehicle Applications: Issues and Recommendations," *IEEE Access*, vol. 6, pp. 19362–19378, 2018.

[16] K. P. Sumarah, M. P. Helios, B. Nuryadin, R. T. Soewono, A. M. Fathoni, R. Deniartiofa, S. A. Saputra, H. Sutriyanto, R. J. Komara, A. Maswan, D. H. Arthanto, H. Pujowidodo, and B. T. Prasetyo, "A Study on the Influence of Torque Variation to Surface Temperature Distribution of Electric Vehicle Battery," *International Conference on Heat Transfer, Energy and Mechanical Innovations*, vol. 31, pp. 1-8, 2022.

[17] H. Pujowidodo, B. T. Prasetyo; R. T. Soewono, et al., "Numerical investigation of heat production in the two-wheeler electric vehicle battery via torque load variation test," *World Electric Vehicle Journal*, vol. 15, no. 1, p. 13, 2024.

[18] W.-Y. Chang, "The state of charge estimating methods for battery: A review," *ISRN Applied Mathematics*, vol. 2013, pp. 1–7, 2013.

[19] M. Zhang and X. Fan, "Review on the state of charge estimation methods for electric vehicle battery," *World Electric Vehicle Journal*, vol. 11, no. 1, p. 23, 2020.

[20] A. PTC, "Event Uncertainty," *Encyclopedia Database System*, vol. 2005, pp. 1068–1068, 2009.

[21] Y. Y. Kee, Y. Asako, T. L. Ken, and N. A. C. Sidik, "Uncertainty of temperature measured by thermocouple," *Journal of Advanced Research in Fluid Mechanics and Thermal Sciences*, vol. 68, no. 1, pp. 54–62, 2020.

[22] V. J. Ovejas and A. Cuadras, "Effects of cycling on lithium-ion battery hysteresis and overvoltage," *Scientific Reports*, vol. 9, no. 1, p. 14875, 2019.